Article

Discovery Medicine 2026; 38(205): 520–530
https://doi.org/10.24976/Discov.Med.202638205.43

ANO1 Facilitates Maladaptive Cardiac Hypertrophy Through Ferroptosis Regulation: A New Therapeutic Axis Revealed

Lina Hou[1], Songjian Xin[2], Wenyao Yu[2,*]

[1]Department of Cardiology, The People's Hospital of Cangnan, 325800 Wenzhou, Zhejiang, China
[2]Department of Rehabilitation, The Second Affiliated Hospital of Wenzhou Medical University, 325500 Wenzhou, Zhejiang, China
*Correspondence: 15858512285@163.com (Wenyao Yu)
Submitted: 14 November 2025 Revised: 2 December 2025 Accepted: 18 December 2025 Published: 20 February 2026

Background: Cardiac hypertrophy is a major risk factor for heart failure, and accumulating evidence suggests that ferroptosis—a form of regulated cell death driven by iron—dependent lipid peroxidation-contributes to its progression. However, the regulatory mechanisms linking cardiac hypertrophy and ferroptosis remain incompletely understood. This study, therefore, aimed to investigate the role of anoctamin 1 (ANO1), a calcium-activated chloride channel, in cardiac hypertrophy and ferroptosis.
Methods: A transverse aortic constriction (TAC) mouse model and angiotensin II (AngII)-stimulated H9c2 cardiomyocytes were used to evaluate ANO1 expression. Loss- and gain-of-function experiments were performed *in vitro* and *in vivo*. Ferroptosis-related markers, oxidative stress indicators, histological changes, and cardiac hypertrophy parameters were assessed by qPCR, Western blotting, immunohistochemistry, and functional assays.
Results: ANO1 expression was significantly elevated in hypertrophic hearts and AngII-treated cardiomyocytes ($p < 0.05$). Silencing ANO1 reduced the expression of the ferroptosis-promoting enzyme Acyl-CoA synthetase long-chain family member 4 (ACSL4), restored solute carrier family 7 member 11 (SLC7A11) and glutathione peroxidase 4 (GPX4) levels ($p < 0.05$), and mitigated oxidative stress and lipid peroxidation, thus leading to improved cell viability and reduced hypertrophy. Conversely, ANO1 overexpression aggravated ferroptosis and oxidative injury ($p < 0.05$), which could be reversed by the ferroptosis inhibitor ferrostatin-1 ($p < 0.05$). *In vivo*, AAV9-mediated ANO1 knockdown attenuated TAC-induced cardiac hypertrophy and ferroptosis ($p < 0.05$), indicating its pathological role.
Conclusion: ANO1 promotes cardiac hypertrophy by enhancing ferroptosis and oxidative stress. Targeting ANO1 may represent a promising therapeutic strategy for preventing or treating pathological cardiac remodeling.

Keywords: ANO1; cardiac hypertrophy; ferroptosis; oxidative stress; angiotensin II; transverse aortic constriction

Introduction

Cardiac hypertrophy is a compensatory response to chronic hemodynamic stress [1], characterized by increased cardiomyocyte size, extracellular matrix remodeling, and elevated expression of hypertrophic markers, such as atrial natriuretic peptide (ANP) and collagen type III (COL3A1) [2,3]. Although initially adaptive, sustained hypertrophy often progresses to heart failure and adverse cardiovascular events [4,5]. Understanding the molecular mechanisms that drive pathological cardiac remodeling is essential for identifying new therapeutic targets.

Ferroptosis is a recently characterized form of regulated cell death, driven by iron-dependent accumulation of lipid peroxides and distinct from apoptosis, necrosis, and autophagy, and closely linked to oxidative stress [6,7]. Emerging evidence implicates ferroptosis in the pathogenesis of cardiovascular diseases, including ischemia-reperfusion injury and pressure overload-induced heart failure [8–10]. However, the upstream regulators of ferroptosis in cardiac hypertrophy remain largely undefined.

Anoctamin 1 (ANO1), also known as TMEM16A, is a calcium-activated chloride channel widely expressed in epithelial and smooth muscle tissues, involved in ion transport, membrane potential regulation, and cellular homeostasis [11–13]. Beyond its established role in promoting tumor proliferation, migration, and oxidative stress adaptation [14–17], recent studies suggest that ANO1 also contributes to cardiovascular function, including vascular tone regulation and cardiac remodeling [12,18]. Given its role in modulating intracellular calcium levels and redox balance, ANO1 may promote ferroptosis in cardiomyocytes by influencing reactive oxygen species (ROS) accumulation and impairing antioxidant defenses, highlighting its potential as a target for interventions aimed at mitigating hypertrophic remodeling and cardiac injury under pathological stress; however the precise mechanisms require further elucidation.

In this study, we investigated the role of ANO1 in cardiac hypertrophy and ferroptosis using both *in vivo* and *in vitro* models. We demonstrate that ANO1 is upregulated in pressure overload-induced hypertrophic hearts and in angiotensin II (AngII)-stimulated cardiomyocytes, and that ANO1 exacerbates cardiac injury by promoting ferroptosis and oxidative stress. These findings provide new insights into the molecular mechanisms underlying cardiac hypertrophy and highlight ANO1 as a potential therapeutic target.

Materials and Methods

Animal Experimental

Male C57BL/6J mice (8–10 weeks old, 22–25 g) were purchased from Beijing SiBeiFu Biotechnology Co., Ltd. (Beijing, China). A total of 36 mice were used in this study, with 6 mice per group. The experiments were conducted in two independent batches. In the first batch, mice were randomly assigned to the Sham or TAC groups (n = 6 per group) to establish the pressure overload model. In the second batch, mice were randomly allocated into four groups: Sham + AAV9-shNC, Sham + AAV9-shANO1, TAC + AAV9-shNC, and TAC + AAV9-shANO1, with 6 mice in each group, to evaluate the effects of ANO1 knockdown *in vivo*. All mice were housed under standard specific pathogen-free (SPF) conditions (22 ± 2 °C, 50–60% humidity, 12-h light/dark cycle) with free access to food and water. Transverse aortic constriction (TAC) surgery was performed to induce pressure overload-mediated cardiac hypertrophy [19]. Mice were anesthetized with 1.5–2.0% isoflurane via a nose cone, and body temperature was maintained at 37 °C using a heating pad throughout the procedure. After endotracheal intubation and mechanical ventilation, a median sternotomy was performed to expose the aortic arch. Aortic constriction was then induced by placing a 7-0 silk suture around the transverse aorta and tying against a 27-gauge needle; the needle was then removed to achieve consistent constriction. Sham-operated mice underwent the same procedure without ligation. Postoperative analgesia was provided using buprenorphine (0.1 mg/kg, subcutaneously). Four weeks after surgery, heart tissues were collected for molecular and histological analyses. The 4-week time point after TAC surgery was selected because it represents the stage of compensated cardiac hypertrophy, during which structural remodeling and functional alterations are clearly detectable but before the transition to overt heart failure, thus allowing stable and interpretable assessment of pressure overload–induced cardiac changes.

To knock down ANO1 *in vivo*, mice were administered adeno-associated virus serotype 9 encoding ANO1-targeting shRNA (AAV9-shANO1) or a negative control (AAV9-shNC), both under the control of the cardiac troponin T (cTNT) promoter (WZ Biosciences Inc., Shandong, China). The sequences used for vector synthesis were as follows: shANO1 (5′-CGAATGCAAGTATGGACTA-3′) and shNC (5′-GCGCGCTTTGTAGGATTCG-3′). A viral suspension (5×10^{11} vector genomes/mouse, 200 µL) was injected via the tail vein. Four weeks after AAV9 administration, mice underwent either TAC or sham surgery and were monitored for an additional 4 weeks before tissue collection. Importantly, AAV9-mediated ANO1 knockdown had been verified beforehand by assessing ANO1 mRNA and protein levels in cardiac tissues.

At the experimental endpoint, mice were euthanized by intraperitoneal overdose administration of pentobarbital sodium (150 mg/kg) followed by cervical dislocation to ensure complete cessation of vital signs. Heart tissues were rapidly excised, rinsed in cold PBS, blotted dry, and weighed. Following heart excision, the right tibia was carefully dissected to obtain an accurate tibial length measurement. The hearts were dissected, and samples were allocated for subsequent analyses. Portions of the left ventricle were fixed in 4% paraformaldehyde for hematoxylin–eosin (HE) staining, FITC-conjugated wheat germ agglutinin (WGA) staining, and immunohistochemistry (IHC) to evaluate cardiac morphology, myocyte cross-sectional area, and ANO1 expression. Additional tissue fractions were snap-frozen in liquid nitrogen for RNA extraction, used to quantify ANO1 mRNA levels, and used for protein extraction for Western blot analysis.

Cell Culture and Treatments

Rat cardiomyoblast H9c2 (2-1) cells (CL-0089) were obtained from Wuhan Pricella Biotechnology Co., Ltd. (Wuhan, China) and cultured in DMEM (11965092, GIBCO, NY, USA) supplemented with 10% fetal bovine serum (A5670501, GIBCO, NY, USA) and 1% penicillin-streptomycin (15070063, GIBCO, NY, USA) at 37 °C in a 5% CO_2 incubator. The cell line was authenticated by short tandem repeat (STR) profiling and was confirmed to show a negative match with all known human cell lines, excluding cross-contamination. Routine mycoplasma PCR testing demonstrated that the cells were free of mycoplasma contamination.

For *in vitro* hypertrophy induction, cells were treated with angiotensin II (AngII, 1 µM; HY-13948, MedchemExpress, Shanghai, China) for 24 or 48 h [20].

Cell Transfection

To manipulate ANO1 expression in H9c2 cells, an ANO1 overexpression plasmid (oe-ANO1) and a short interfering RNA targeting ANO1 (si-ANO1) were both synthesized by Sangon Biotech Co., Ltd. (Shanghai, China). The coding sequence used for ANO1 overexpression (oe-ANO1) was based on the full-length rat ANO1 (TMEM16A) sequence (NCBI Reference Sequence: NM_001107564.1). The siRNA sequence targeting rat ANO1 (si-ANO1)

Table 1. Primer sequence.

Gene	Primer sequence (5′-3′)
ANO1 (mouse)	F: CTCGTGGTCATCATTCTGCTGG R: GCCTTGAAGGTTAGCCTCTCCT
ANO1 (rat)	F: CCCAGAGCAGAGTATGAAGCC R: ACATTCCGGCGCTTCTCTTT
GAPDH (mouse)	F: CATCACTGCCACCCAGAAGACTG R: ATGCCAGTGAGCTTCCCGTTCAG
GAPDH (rat)	F: GACAACTTTGGCATCGTGGA R: ATGCAGGGATGATGTTCTGG

ANO1, anoctamin 1; *GAPDH*, glyceraldehyde-3-phosphate dehydrogenase.

was 5′-GGUGUACCAUCACAAGAGAGC-3′. The negative control siRNA (si-NC) sequence was 5′-UUCUCCGAACGUGUCACGU-3′. The negative control plasmid (oe-NC) contained no coding insert and corresponded to the empty pcDNA3.1(+) vector. For transfection, 2.5 µg of pcDNA3.1-ANO1 or control vector (oe-NC), and 2 µg of si-ANO1 or negative control siRNA (si-NC), were introduced into 5×10^5 cells using Lipofectamine 3000 (L3000001, Invitrogen, CA, USA) according to the manufacturer's instructions. Where indicated, cells were treated with ferrostatin-1 (Fer-1, 10 µM; HY-100579, MedchemExpress, Shanghai, China) for ferroptosis inhibition based on the perious study reporting effective suppression of ferroptosis at this concentration [21], and the treatment was maintained for 24 h.

Quantitative Real-Time PCR

Total RNA was extracted from heart tissues or H9c2 cells using TRIzol reagent (15596026CN, Invitrogen, CA, USA). cDNA was synthesized using a reverse transcription kit (6210A, Takara, Shiga, Japan), and quantitative PCR was performed with SYBR Green PCR Master Mix (4367659, Thermo Fisher Scientific, MA, USA) on an Applied Biosystems QuantStudio 5 real-time PCR system (Thermo Fisher Scientific, MA, USA). Each 20 µL qPCR reaction was prepared with 10 µL SYBR Green Master Mix, 0.4 µL each of forward and reverse primer (10 µM), 2 µL cDNA template (equivalent to ~10–50 ng RNA), and nuclease-free water to adjust the volume to 20 µL. The primer sequences used for qPCR are listed in Table 1 . The qPCR cycling program was: 95 °C for 3 min; 40 cycles of 95 °C for 10 s and 60 °C for 30 s; followed by a melt-curve analysis to verify single specific products. Relative mRNA expression was calculated using the $2^{-\Delta\Delta Ct}$ method with GAPDH as an internal control.

Western Blotting

Proteins were extracted from treated H9c2 cells and treated mouse heart tissues using RIPA buffer (R488105, Aladdin, Shanghai, China) containing protease inhibitors (P665818, Aladdin, Shanghai, China), and quantified using the BCA assay (PP102-01, Beyotime, Shanghai, China). Equal amounts of protein were separated by SDS-PAGE and transferred onto PVDF membranes. After blocking, membranes were incubated overnight at 4 °C with primary antibodies against ANO1 (BA3464-2, Bosterbio, Wuhan, China), ANP (1:2000, 27426-1-AP, Proteintech, Wuhan, China), BNP (1:500, ab19645, Abcam, Cambridge, UK), COL3A1 (1:300, 22734-1-AP, Proteintech, Wuhan, China), ACSL4 (1:5000, 22401-1-AP, Proteintech, Wuhan, China), SLC7A11 (1:1000, ab307601, Abcam, Cambridge, UK), GPX4 (1:1000, 67763-1-Ig, Proteintech, Wuhan, China), and GAPDH (1:50,000, 60004-1-Ig, Proteintech, Wuhan, China), followed by HRP-conjugated secondary antibodies (1:2000, SA00001-1, SA00001-2, Proteintech, Wuhan, China). Protein bands were visualized using enhanced chemiluminescence reagents and imaged using a Chemi-Doc™ MP Imaging System (Bio-Rad, CA, USA). Densitometric analysis was performed using ImageJ software (version 1.53; National Institutes of Health, Bethesda, MD, USA).

Histological Analysis

Mouse heart tissues were harvested immediately after euthanasia and rinsed in pre-cooled PBS (C0221A; Beyotime, Shanghai, China) to remove residual blood. For paraffin embedding, tissues were fixed in 4% paraformaldehyde (P1110; Solarbio, Beijing, China) for 24–48 h at room temperature, dehydrated through graded ethanol, cleared in xylene (X822031; Macklin, Shanghai, China), and embedded in paraffin. Sections were cut at 5 µm thickness using a rotary microtome (RM2235; Leica, Germany). HE staining was subsequently performed using a commercial kit (HE Staining Kit, G1120; Solarbio, Beijing, China) following the manufacturer's protocol.

For membrane labeling, cardiac tissues were embedded in optimal cutting temperature compound (4583; Sakura Finetek, USA) and cryosectioned at 8–10 µm using a cryostat (CM1950; Leica, Germany). Sections were incubated with FITC-conjugated wheat germ agglutinin (WGA-FITC, GTX01502; GeneTex, USA) at 10 µg/mL for 30 min at room temperature in the dark, followed by washing with PBS. Slides were mounted using an antifade fluorescence mounting medium (P0126; Beyotime, China). Images were captured using a fluorescence microscope (Axio Observer 7; Zeiss, Germany). Quantification of cardiomyocyte cross-sectional area and fluorescence intensity was performed using ImageJ software.

Immunohistochemical Staining

For IHC, paraffin-embedded mouse heart tissue sections were deparaffinized, rehydrated, and blocked with phosphate-buffered saline (PBS) containing 5% normal goat serum and 1% bovine serum albumin for 1 hour at room temperature. The sections were then incubated

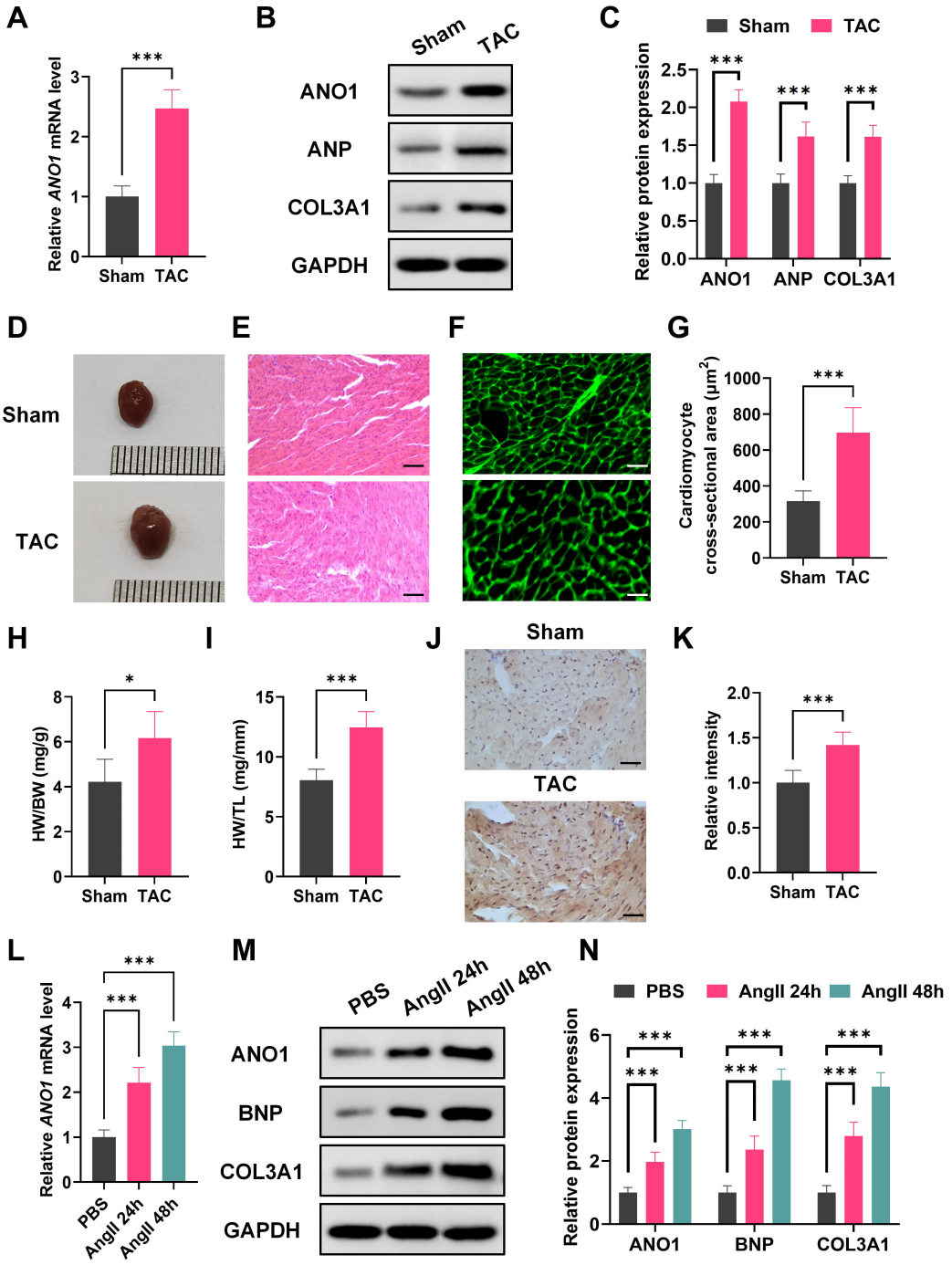

Fig. 1. ANO1 is significantly upregulated in TAC-induced cardiac hypertrophy and AngII-stimulated cardiomyocytes. (A) mRNA expression levels of ANO1 in heart tissues from Sham and TAC mice. (B,C) Protein expression of ANO1, ANP, and COL3A1 in heart tissues from Sham and TAC mice determined by Western blotting. (D) Macroscopic view of hearts from Sham and TAC groups. Histological staining of heart tissues: (E) HE staining (scale bar = 50 μm) and (F) FITC-conjugated WGA staining (scale bar = 100 μm). (G) Quantification of cardiomyocyte cross-sectional area based on WGA staining. Quantification of cardiac hypertrophy by (H) HW/BW ratio and (I) HW/TL ratio. (J,K) Immunohistochemistry staining of ANO1 in ventricular sections from Sham and TAC mice (scale bar = 100 μm). (L) mRNA expression of ANO1 in H9c2 cells treated with PBS, AngII for 24 h, and AngII for 48 h. (M,N) Western blot analysis of ANO1, BNP, and COL3A1 in H9c2 cells under the indicated treatments. For animal experiments, each group included n = 6 mice, and for cell-based experiments, all assays were performed in triplicate (n = 3). * $p < 0.05$, *** $p < 0.001$. ANO1, anoctamin 1; TAC, transverse aortic constriction; AngII, angiotensin II; ANP, atrial natriuretic peptide; COL3A1, collagen type III; HE, hematoxylin–eosin; FITC, fluorescein isothiocyanate; WGA, wheat germ agglutinin; PBS, phosphate-buffered saline; BNP, brain natriuretic peptide; HW, heart weight; BW, body weight; TL, tibia length.

overnight at 4 °C with primary antibody against ANO1 (BA3464-2, Bosterbio, Wuhan, China) in a humidified chamber. On the following day, sections were incubated with HRP-conjugated anti-rabbit secondary antibody (ab150077, Abcam, Cambridge, UK) for 1 h at room temperature. Quantitative analysis of staining intensity was conducted using Image-Pro Plus software (version 6.0; Media Cybernetics, Rockville, MD, USA).

Biochemical Assays

Oxidative stress markers were assessed using commercial kits (Beyotime, Shanghai, China). All biochemical assays were performed using homogenates of mouse heart tissue and lysates of H9c2 cells. Superoxide dismutase (SOD) activity was measured using the SOD Assay Kit (S0109), following the manufacturer's protocol, where the absorbance was detected at 560 nm. Malondialdehyde (MDA) levels were determined using the Lipid Peroxidation MDA Assay Kit (S0131S) with absorbance measured at 532 nm. The glutathione/glutathione disulfide ratio (GSH/GSSG) was quantified using the GSH/GSSG Assay Kit (S0053) with measurement at 412 nm. The concentration of 4-hydroxynonenal (4-HNE) was measured using a commercial ELISA kit (E-EL-0128, Elabscience, Wuhan, China). After sample incubation and reagent processing, the absorbance was measured at 450 nm using a microplate reader (SpectraMax i3x; Molecular Devices, USA). Quantification for each assay was performed based on standard curves generated according to the manufacturer's instructions.

ROS Detection

Intracellular reactive oxygen species (ROS) levels were measured using a Reactive Oxygen Species Assay Kit (S0034S; Beyotime, Shanghai, China) following the manufacturer's protocol. Briefly, treated cells were incubated with 10 μM 2′,7′-dichlorofluorescein diacetate (DCFH-DA) at 37 °C for 30 minutes in the dark. After incubation, cells were washed with PBS, and fluorescence was either observed under a fluorescence microscope (BX63, Olympus, Japan). ROS fluorescence intensity was quantified using ImageJ software, and statistical analysis of fluorescence intensity was performed by averaging the mean fluorescence values from at least five random fields per sample.

Statistical Analysis

All statistical analyses and graph generation were performed using GraphPad Prism 9.5 (GraphPad Software, San Diego, CA, USA). Data were presented as mean ± standard deviation (SD). Comparisons between two groups were performed using unpaired Student's *t*-test, and multiple group comparisons were conducted using one-way ANOVA followed by Tukey's post hoc test. Statistical significance was defined as $p < 0.05$.

Results

ANO1 Expression Is Elevated in TAC-Induced Cardiac Hypertrophy and AngII-Stimulated H9c2 Cells

To investigate the potential involvement of ANO1 in cardiac hypertrophy, we first examined its expression in a pressure overload-induced hypertrophic mouse model established by transverse aortic constriction (TAC). Quantitative PCR revealed a significant upregulation of ANO1 mRNA in the hearts of TAC mice compared to Sham controls (Fig. 1A, $p < 0.05$). Consistently, Western blot analysis demonstrated markedly increased protein levels of ANO1, as well as the hypertrophic markers ANP and COL3A1, in TAC heart tissues (Fig. 1B,C, $p < 0.05$). Morphological analysis showed pronounced cardiac enlargement in TAC mice (Fig. 1D), which was further supported by histological evidence of myocardial hypertrophy and disorganization via HE staining (Fig. 1E) and increased cardiomyocyte cross-sectional area by WGA staining (Fig. 1F,G). Quantitative measurements indicated significant increases in HW/BW and HW/TL ratios in TAC mice (Fig. 1H,I, $p < 0.05$). Moreover, immunohistochemical staining confirmed enhanced ANO1 expression in the ventricular tissues of TAC mice (Fig. 1J,K, $p < 0.05$).

To further validate these findings *in vitro*, H9c2 cells were treated with AngII for 24 h and 48 h. Compared to PBS-treated controls, both ANO1 mRNA and protein levels were significantly elevated following AngII stimulation, in parallel with increased expression of BNP and COL3A1 (Fig. 1L–N, $p < 0.05$). These results collectively indicate that ANO1 is markedly upregulated during cardiac hypertrophy both *in vivo* and *in vitro*.

Silencing ANO1 Alleviates AngII-Induced Oxidative Stress and Ferroptosis in H9c2 Cardiomyocytes

To elucidate the functional role of ANO1 in cardiomyocyte injury, siRNA-mediated knockdown of ANO1 was performed in H9c2 cells. Quantitative PCR and Western blot analyses confirmed that ANO1 expression was significantly reduced at both mRNA and protein levels in the si-ANO1 group compared to the control and si-NC groups (Fig. 2A–C, $p < 0.05$). Under AngII stimulation, ANO1 knockdown notably reversed the upregulation of hypertrophic markers BNP and COL3A1, as well as the ferroptosis-related enzyme ACSL4 ($p < 0.05$). In contrast, under AngII stimulation, levels of SLC7A11 and GPX4, key negative regulators of ferroptosis, were preserved in the si-ANO1 group (Fig. 2D,E, $p < 0.05$).

Functionally, oxidative stress indicators were markedly improved in the AngII-si-ANO1 group: SOD activity was restored (Fig. 2F, $p < 0.05$), the GSH/GSSG ratio was increased (Fig. 2G, $p < 0.05$), and MDA levels were reduced (Fig. 2H, $p < 0.05$), indicating alleviation of lipid peroxidation. Fluorescence staining further revealed

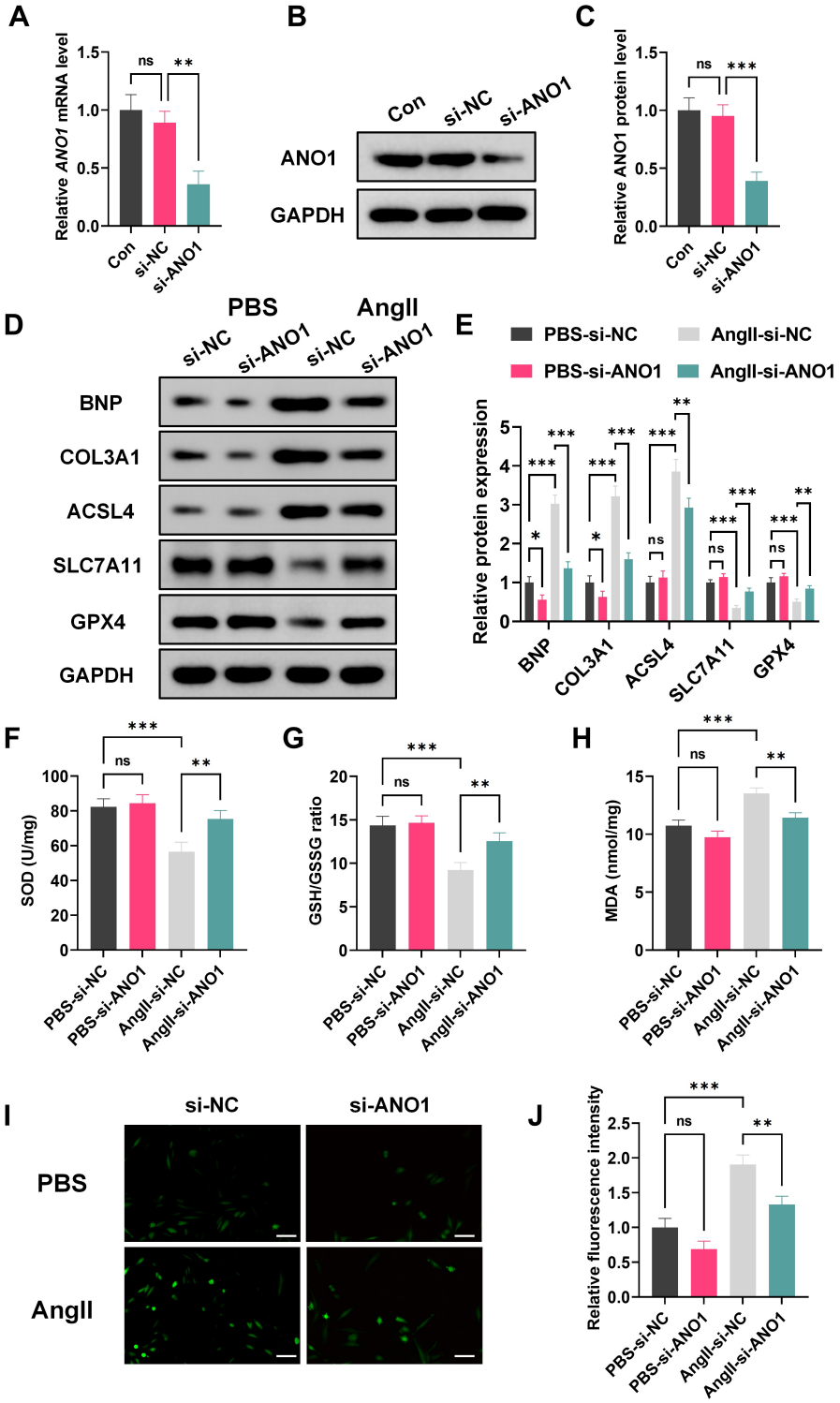

Fig. 2. Silencing ANO1 attenuates AngII-induced oxidative stress and ferroptosis in H9c2 cardiomyocytes. (A) mRNA expression levels of *ANO1* in con, si-NC, and si-ANO1 transfected H9c2 cells. (B,C) Western blot analysis of ANO1 protein levels in con, si-NC, and si-ANO1 groups. (D,E) Western blot analysis of BNP, COL3A1, ACSL4, SLC7A11, and GPX4 expression in different treated H9c2 cells. (F–H) Levels of oxidative stress-related indicators: (F) SOD, (G) GSH/GSSG ratio, and (H) MDA in PBS-si-NC, PBS-si-ANO1, AngII-si-NC, and AngII-si-ANO1 groups. (I,J) Intracellular ROS levels determined by fluorescence staining (scale bar = 50 µm). n = 3; ns, $p > 0.05$, * $p < 0.05$, ** $p < 0.01$, *** $p < 0.001$. si-NC, negative control siRNA; ACSL4, Acyl-CoA synthetase long-chain family member 4; SLC7A11, solute carrier family 7 member 11; GPX4, glutathione peroxidase 4; GSH, glutathione; GSSG, glutathione disulfide; MDA, malondialdehyde; ROS, reactive oxygen species; ns, not significant.

that ANO1 knockdown attenuated the AngII-induced accumulation of ROS, which was quantitatively confirmed by fluorescence intensity analysis (Fig. 2I,J, $p < 0.05$). These results suggest that ANO1 promotes AngII-induced oxidative stress and ferroptosis, and its inhibition confers protective effects on cardiomyocytes.

ANO1 Overexpression Exacerbates Ferroptosis and Oxidative Stress in H9c2 Cells, Which Is Mitigated by Fer-1 Treatment

To further confirm the role of ANO1 in ferroptosis, we overexpressed ANO1 in H9c2 cells, followed by AngII stimulation, with or without treatment of the ferroptosis inhibitor Fer-1. Western blot results showed that ANO1 overexpression under AngII treatment markedly increased the levels of ACSL4 ($p < 0.05$), a key pro-ferroptotic enzyme, while simultaneously reducing the expression of SLC7A11 and GPX4 ($p < 0.05$), two critical anti-ferroptotic regulators. These effects were substantially reversed by co-treatment with Fer-1 (Fig. 3A,B), indicating the involvement of ferroptotic mechanisms.

In addition, ANO1 overexpression combined with AngII stimulation significantly decreased antioxidant enzyme activity, as evidenced by reduced SOD levels (Fig. 3C, $p < 0.05$) and a lowered GSH/GSSG ratio (Fig. 3D, $p < 0.05$), while increasing MDA content (Fig. 3E, $p < 0.05$), a hallmark of lipid peroxidation. In addition, ROS accumulation was markedly elevated in the oe-ANO1 group, as shown by fluorescence staining, whereas Fer-1 treatment effectively suppressed ROS generation (Fig. 3F,G, $p < 0.05$).

Silencing ANO1 Mitigates TAC-Induced Cardiac Hypertrophy and Ferroptosis In Vivo

To evaluate the *in vivo* relevance of ANO1 in pressure overload-induced cardiac remodeling, ANO1 was silenced via AAV9-mediated delivery of shRNA in a TAC mouse model. Macroscopic examination revealed that hearts from TAC-shNC mice exhibited pronounced hypertrophic enlargement, whereas ANO1 knockdown (TAC-shANO1) attenuated this phenotype (Fig. 4A). FITC-conjugated WGA staining showed a decreased cross-sectional area of cardiomyocytes in TAC-shANO1 hearts compared to TAC-shNC controls (Fig. 4B,C, $p < 0.05$). Consistently, quantitative analysis revealed that both HW/BW and HW/TL ratios were significantly reduced following ANO1 silencing in TAC mice (Fig. 4D,E, $p < 0.05$).

To assess oxidative stress and ferroptosis *in vivo*, we measured serum levels of 4-HNE and MDA, both of which were markedly elevated in TAC-shNC mice but significantly decreased in TAC-shANO1 mice (Fig. 4F,G, $p < 0.05$). Western blot analysis of cardiac tissues showed that TAC-induced upregulation of ANO1 and the pro-ferroptotic marker ACSL4 was significantly suppressed by ANO1 knockdown, while the expression of anti-ferroptotic proteins SLC7A11 and GPX4 was restored (Fig. 4H,I, $p < 0.05$).

Discussion

Cardiac hypertrophy, as a compensatory response to hemodynamic stress, is a critical pathological basis for heart failure [22]. Traditionally considered an adaptive mechanism, sustained hypertrophic remodeling leads to myocardial dysfunction and adverse structural changes. While its progression is regulated by multiple molecular and cellular pathways, recent evidence has implicated ferroptosis, a form of regulated cell death characterized by lipid peroxidation, in the development of cardiac dysfunction [23,24]. In this study, we identified ANO1, a calcium-activated chloride channel, as a key modulator of cardiac hypertrophy and ferroptosis. Our findings demonstrate that ANO1 is significantly upregulated in the myocardium of TAC-induced hypertrophic mice and in AngII-stimulated H9c2 cells, suggesting its involvement in pathological remodeling. Notably, previous studies also reported ANO1 upregulation in injured cardiac tissues; however, its functional consequences appear to be context-dependent. For instance, Gao *et al*. [25] found that ANO1 increased in neonatal rat cardiac fibroblasts after hypoxia and in myocardial infarction tissues, where its overexpression reduced fibrosis by suppressing the TGF-β/Smad3 pathway. In contrast, our study demonstrates that ANO1 upregulation in cardiomyocytes promotes oxidative imbalance and ferroptosis, thereby aggravating hypertrophic remodeling. These differences may reflect cell-type–specific functions (fibroblasts vs. cardiomyocytes), distinct pathological contexts (ischemic fibrosis vs. pressure overload hypertrophy), and divergent downstream pathways (TGF-β/Smad3 inhibition vs. ACSL4/SLC7A11/GPX4-mediated ferroptosis regulation).

Mechanistically, silencing ANO1 ameliorated AngII-induced oxidative stress, restored redox homeostasis, as evidenced by the normalization of SOD activity, GSH/GSSG ratio, and the reduction of MDA and ROS levels. These findings imply that ANO1 may disrupt the intracellular antioxidant system, thereby sensitizing cardiomyocytes to ferroptotic injury. This redox imbalance may prime cardiomyocytes for ferroptosis by promoting lipid peroxidation and depleting endogenous antioxidant capacity. In line with this, ANO1 knockdown suppressed the expression of ACSL4, a pro-ferroptotic enzyme, while upregulating SLC7A11 and GPX4, two critical ferroptosis-inhibiting proteins. These results suggest that ANO1 promotes ferroptosis in cardiomyocytes, likely through dysregulation of redox balance and lipid metabolism. This is consistent with the established model in which downregulation of SLC7A11 or GPX4 and upregulation of ACSL4 sensitize cardiomyocytes to ferroptosis under stress conditions [26].

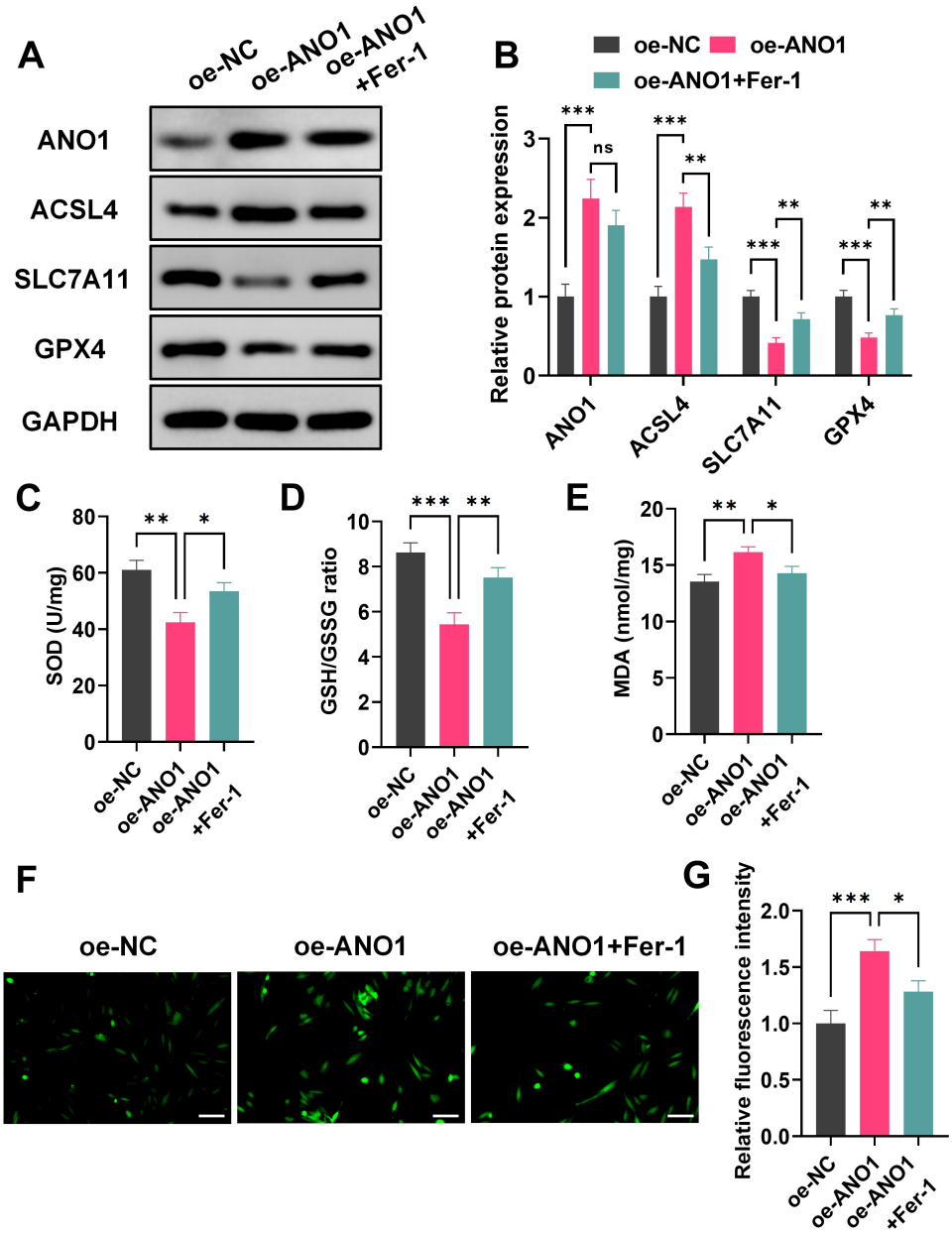

Fig. 3. ANO1 overexpression promotes ferroptosis in H9c2 cardiomyocytes, which is reversed by Fer-1 treatment. (A,B) Western blot analysis of ANO1, ACSL4, SLC7A11, and GPX4 expression in oe-NC, oe-ANO1, and oe-ANO1 + Fer-1 treated H9c2 cells. (C–E) Assessment of oxidative stress-related parameters in different treated H9c2 cells: (C) SOD levels, (D) GSH/GSSG ratio, and (E) MDA levels. (F,G) Intracellular ROS levels assessed by fluorescence staining (scale bar = 50 μm). n = 3; ns, $p > 0.05$, * $p < 0.05$, ** $p < 0.01$, *** $p < 0.001$. Fer-1, ferrostatin-1; SOD, superoxide dismutase.

Conversely, ANO1 overexpression in AngII-treated H9c2 cells exacerbated ferroptotic cell death, as indicated by enhanced ACSL4 expression, depleted SLC7A11 and GPX4 levels, increased ROS accumulation, and reduced antioxidant capacity. This bidirectional effect positions ANO1 as a molecular switch that governs cardiomyocyte susceptibility to ferroptosis. Notably, treatment with the ferroptosis inhibitor Fer-1 reversed these deleterious effects, reinforcing the role of ANO1 in ferroptosis regulation. Similarly, pharmacological inhibition of ferroptosis has been shown to mitigate cardiomyocyte death and myocardial injury in iron overload or ischemia/reperfusion models, supporting the therapeutic relevance of targeting ferroptosis in heart disease [27]. This bidirectional regulatory pattern suggests that ANO1 may serve as a molecular switch modulating cardiomyocyte susceptibility to redox-driven cell death.

Importantly, *in vivo* silencing of ANO1 using AAV9-shRNA significantly attenuated cardiac hypertrophy and ferroptosis in TAC mice, as evidenced by improved car-

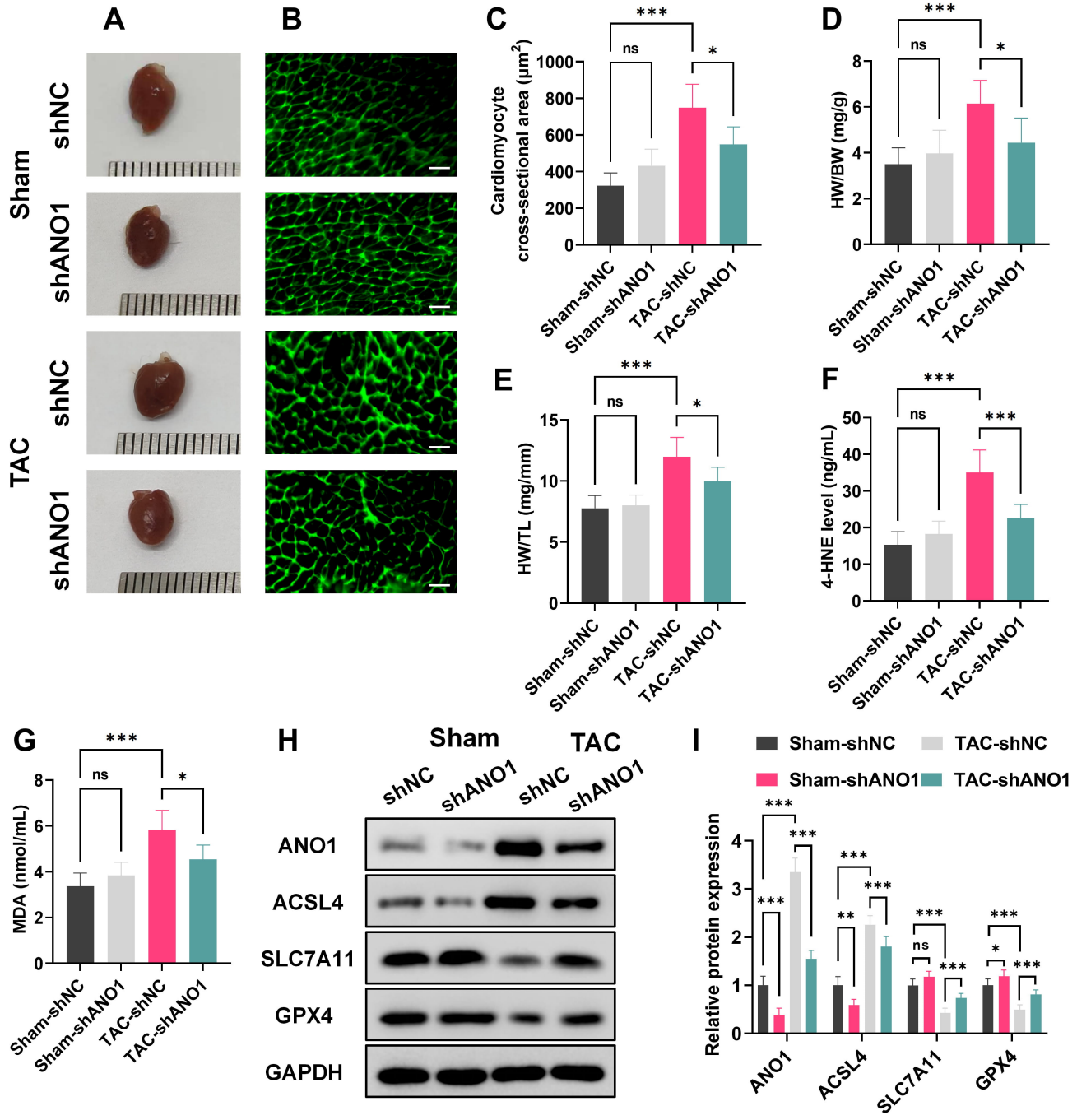

Fig. 4. Silencing ANO1 alleviates TAC-induced cardiac hypertrophy and ferroptosis *in vivo*. (A) Macroscopic view of hearts from Sham-shNC, Sham-shANO1, TAC-shNC, and TAC-shANO1 mice. Histological staining of cardiac tissues: (B) FITC-conjugated WGA staining (scale bar = 100 μm). (C) Quantification of cardiomyocyte cross-sectional area based on WGA staining. Quantification of cardiac hypertrophy by (D) HW/BW ratio and (E) HW/TL ratio. Serum levels of oxidative stress markers: (F) 4-HNE and (G) MDA. (H,I) Western blot analysis of ANO1, ACSL4, SLC7A11, and GPX4 expression in cardiac tissues from the four groups. n = 6; ns, $p > 0.05$, * $p < 0.05$, ** $p < 0.01$, *** $p < 0.001$. HW, heart weight; BW, body weight; TL, tibia length; 4-HNE, 4-hydroxynonenal.

diac structure, reduced expression of hypertrophic markers, and decreased systemic oxidative stress, reflected by lower serum levels of 4-HNE and MDA. These protective effects were accompanied by favorable changes in ferroptosis-related protein expression, consistent with *in vitro* findings. These results suggest that the pro-ferroptotic role of ANO1 extends beyond the cellular level to impact whole-organism physiology, highlighting its broader pathological significance. This finding aligns with the recent study which demonstrated that interventions restoring antioxidant defenses (e.g., upregulating SLC7A11/GPX4 axis or inhibiting lipid peroxidation) can prevent cardiac remodeling and

dysfunction in models of pressure overload or metabolic stress [28]. The simultaneous improvement in both structural remodeling and biochemical indicators further underscores ANO1's integrative role in mediating stress-induced cardiac injury.

While the precise upstream triggers of ANO1 activation under pressure overload remain to be elucidated, it is plausible that neurohormonal factors or mechanical stress may drive its upregulation. Further studies should investigate whether ANO1 interacts with other ion channels or redox-sensitive signaling pathways to orchestrate cardiomyocyte fate under chronic stress. Moreover, given the critical role of the SLC7A11/GPX4 axis and lipid metabolism enzymes (e.g., ACSL4) in cardiac ferroptosis, future research should investigate whether ANO1 modulates ferroptosis through direct regulation of these pathways or via upstream redox-sensitive signaling—a hypothesis supported by accumulating evidence in cardiovascular ferroptosis research. It should be noted that H9c2 cells are rat cardiomyoblasts and may not fully reflect the physiology of adult cardiomyocytes, therefore some marker changes, such as ANP, require elucidation in primary or adult cardiomyocyte models.

Conclusion

This study identifies ANO1 as a key contributor to cardiac hypertrophy and ferroptosis. ANO1 expression is elevated in hypertrophic hearts and AngII-stimulated cardiomyocytes, promoting oxidative stress and lipid peroxidation through upregulation of ACSL4 and downregulation of SLC7A11 and GPX4. ANO1 knockdown alleviates cardiac hypertrophy and ferroptosis both *in vitro* and *in vivo*, while its overexpression exacerbates these effects. These findings suggest that ANO1 may serve as a potential therapeutic target for preventing pathological cardiac remodeling.

Availability of Data and Materials

The datasets used or analyzed during the current study are available from the corresponding author upon reasonable request.

Author Contributions

LH contributed to the study conception and design, data acquisition, and manuscript drafting. SX was responsible for data analysis, interpretation of results, and critical revision of the manuscript. WY participated in experimental implementation, data validation, and manuscript editing. All authors read and approved the final manuscript. All authors have participated sufficiently in the work to take public responsibility for appropriate portions of the content and agreed to be accountable for all aspects of the work in ensuring that questions related to its accuracy or integrity.

Ethics Approval and Consent to Participate

All animal experiments were approved and conducted in accordance with the guidelines established by the Institutional Animal Care Committee of The People's Hospital of Cangnan (Approval No. 2025026).

Acknowledgment

Not applicable.

Funding

This work was supported by the Science and Technology Program of Wenzhou (YC20250735).

Conflict of Interest

The authors declare no conflict of interest.

References

[1] Frey N, Olson EN. Cardiac hypertrophy: the good, the bad, and the ugly. Annual Review of Physiology. 2003; 65: 45–79. https://doi.org/10.1146/annurev.physiol.65.092101.142243.

[2] Rohini A, Agrawal N, Koyani CN, Singh R. Molecular targets and regulators of cardiac hypertrophy. Pharmacological Research. 2010; 61: 269–280. https://doi.org/10.1016/j.phrs.2009.11.012.

[3] Carreño JE, Apablaza F, Ocaranza MP, Jalil JE. Cardiac hypertrophy: molecular and cellular events. Revista Espanola De Cardiologia. 2006; 59: 473–486.

[4] Tham YK, Bernardo BC, Ooi JYY, Weeks KL, McMullen JR. Pathophysiology of cardiac hypertrophy and heart failure: signaling pathways and novel therapeutic targets. Archives of Toxicology. 2015; 89: 1401–1438. https://doi.org/10.1007/s00204-015-1477-x.

[5] Distefano G, Sciacca P. Molecular pathogenesis of myocardial remodeling and new potential therapeutic targets in chronic heart failure. Italian Journal of Pediatrics. 2012; 38: 41. https://doi.org/10.1186/1824-7288-38-41.

[6] Bi X, Wu X, Chen J, Li X, Lin Y, Yu Y, *et al*. Characterization of ferroptosis-triggered pyroptotic signaling in heart failure. Signal Transduction and Targeted Therapy. 2024; 9: 257. https://doi.org/10.1038/s41392-024-01962-6.

[7] Ru Q, Li Y, Chen L, Wu Y, Min J, Wang F. Iron homeostasis and ferroptosis in human diseases: mechanisms and therapeutic prospects. Signal Transduction and Targeted Therapy. 2024; 9: 271. https://doi.org/10.1038/s41392-024-01969-z.

[8] Zhang M, Guan X, Dong Z, Yang C, Xiong C, Cheng W, *et al*. Targeting Zfp36 to combat cardiac hypertrophy: Insights into ferroptosis pathways. Clinical and Translational Medicine. 2025; 15: e70247. https://doi.org/10.1002/ctm2.70247.

[9] Zhang CH, Yan YJ, Luo Q. The molecular mechanisms and potential drug targets of ferroptosis in myocardial ischemia-reperfusion injury. Life Sciences. 2024; 340: 122439. https://doi.org/10.1016/j.lfs.2024.122439.

[10] Cruz-Gregorio A. Targeting Ferroptosis via Mitochondria Dynamics in Myocardial Ischemia/Reperfusion Injury. Discovery Medicine. 2025; 37: 816–827. https://doi.org/10.24976/Discov.Med.202537196.72.

[11] Genovese M, Galietta LJV. Anoctamin pharmacology. Cell Cal-

cium. 2024; 121: 102905. https://doi.org/10.1016/j.ceca.2024.102905.

[12] Arreola J, Pérez-Cornejo P, Segura-Covarrubias G, Corral-Fernández N, León-Aparicio D, Guzmán-Hernández ML. Function and Regulation of the Calcium-Activated Chloride Channel Anoctamin 1 (TMEM16A). Handbook of Experimental Pharmacology. 2024; 283: 101–151. https://doi.org/10.1007/164_2022_592.

[13] Sun W, Guo S, Li Y, Li J, Liu C, Chen Y, *et al*. Anoctamin 1 controls bone resorption by coupling Cl^- channel activation with RANKL-RANK signaling transduction. Nature Communications. 2022; 13: 2899. https://doi.org/10.1038/s41467-022-30625-9.

[14] Hu Y, Zhang Y, He J, Rao H, Zhang D, Shen Z, *et al*. ANO1: central role and clinical significance in non-neoplastic and neoplastic diseases. Frontiers in Immunology. 2025; 16: 1570333. https://doi.org/10.3389/fimmu.2025.1570333.

[15] Li X, Wang Y, Zhang L, Yao S, Liu Q, Jin H, *et al*. The role of anoctamin 1 in liver disease. Journal of Cellular and Molecular Medicine. 2024; 28: e18320. https://doi.org/10.1111/jcmm.18320.

[16] Zhang X, Lin J, Xu H, Zhou Y, Mu Z, Shi R, *et al*. Mechanism of action and therapeutic value of anoctamin-1 in gastrointestinal cancers. Frontiers in Immunology. 2025; 16: 1599100. https://doi.org/10.3389/fimmu.2025.1599100.

[17] Seo Y, Lee S, Das R, Jeong SB, Park CS, Kim M, *et al*. Vitexicarpin suppresses colorectal and non-small cell lung cancer via selective inhibition of Anoctamin 1. Frontiers in Pharmacology. 2025; 16: 1557193. https://doi.org/10.3389/fphar.2025.1557193.

[18] Jimenez C, Hawn MB, Akin E, Leblanc N. Translational potential of targeting Anoctamin-1-Encoded Calcium-Activated chloride channels in hypertension. Biochemical Pharmacology. 2022; 206: 115320. https://doi.org/10.1016/j.bcp.2022.115320.

[19] Tavakoli R, Nemska S, Jamshidi P, Gassmann M, Frossard N. Technique of Minimally Invasive Transverse Aortic Constriction in Mice for Induction of Left Ventricular Hypertrophy. Journal of Visualized Experiments. 2017; 56231. https://doi.org/10.3791/56231.

[20] Syed AM, Kundu S, Ram C, Kulhari U, Kumar A, Mugale MN, *et al*. Up-regulation of Nrf2/HO-1 and inhibition of TGF-β1/Smad2/3 signaling axis by daphnetin alleviates transverse aortic constriction-induced cardiac remodeling in mice. Free Radical Biology & Medicine. 2022; 186: 17–30. https://doi.org/10.1016/j.freeradbiomed.2022.04.019.

[21] Wu YT, Zhang GY, Hua Y, Fan HJ, Han X, Xu HL, *et al*. Ferrostatin-1 suppresses cardiomyocyte ferroptosis after myocardial infarction by activating Nrf2 signaling. The Journal of Pharmacy and Pharmacology. 2023; 75: 1467–1477. https://doi.org/10.1093/jpp/rgad080.

[22] Gao W, Guo N, Yan H, Zhao S, Sun Y, Chen Z. Mycn ameliorates cardiac hypertrophy-induced heart failure in mice by mediating the USP2/JUP/Akt/β-catenin cascade. BMC Cardiovascular Disorders. 2024; 24: 82. https://doi.org/10.1186/s12872-024-03748-8.

[23] Jin S, Wang H, Zhang X, Song M, Liu B, Sun W. Emerging regulatory mechanisms in cardiovascular disease: Ferroptosis. Biomedicine & Pharmacotherapy. 2024; 174: 116457. https://doi.org/10.1016/j.biopha.2024.116457.

[24] Fang W, Xie S, Deng W. Ferroptosis mechanisms and regulations in cardiovascular diseases in the past, present, and future. Cell Biology and Toxicology. 2024; 40: 17. https://doi.org/10.1007/s10565-024-09853-w.

[25] Gao Y, Zhang YM, Qian LJ, Chu M, Hong J, Xu D. ANO1 inhibits cardiac fibrosis after myocardial infraction via TGF-β/smad3 pathway. Scientific Reports. 2017; 7: 2355. https://doi.org/10.1038/s41598-017-02585-4.

[26] Xie LH, Fefelova N, Pamarthi SH, Gwathmey JK. Molecular Mechanisms of Ferroptosis and Relevance to Cardiovascular Disease. Cells. 2022; 11: 2726. https://doi.org/10.3390/cells11172726.

[27] Xiao D, Chang W, Ao X, Ye L, Wu W, Song L, *et al*. Parkin inhibits iron overload-induced cardiomyocyte ferroptosis by ubiquitinating ACSL4 and modulating PUFA-phospholipids metabolism. Acta Pharmaceutica Sinica. B. 2025; 15: 1589–1607. https://doi.org/10.1016/j.apsb.2024.12.027.

[28] Wei X, Fan X, Chai W, Xiao J, Zhao J, He A, *et al*. Dietary limonin ameliorates heart failure with preserved ejection fraction by targeting ferroptosis *via* modulation of the Nrf2/SLC7A11/GPX4 axis: an integrated transcriptomics and metabolomics analysis. Food & Function. 2025; 16: 3553–3574. https://doi.org/10.1039/d5fo00475f.